2 Experimental Techniques

A discussion follows on the various experimental techniques used for ultrasonic investigations. In the last few decades, considerable progress has been made in the field of high resolution sound velocity and sound attenuation measurements. A wide variety of different methods are used in this field. A distinction can be made between techniques which use transducers and others which are contact free methods. To the latter ones belong the vibrating reed technique and the Brillouin scattering. Numerous books and review articles describe all these topics.

In the low frequency regime, where the sound wavelength is of the dimension of the specimen, the elastic moduli (Young's modulus E and shear modulus G) can be determined by a c.w. resonance method or by measuring flexural and torsional oscillations. At audio frequencies the vibrating reed technique is most frequently applied (Read et al. [2.1]). A brief account of this technique is given in Sect. 2.2.5. In the ultrasonic regime, the elastic constants c_{ij} can be determined by using pulse or c.w. techniques (Truell et al. [2.2], Bolef and Miller [2.3], Fuller et al. [2.4]). The most widely used method to measure sound velocity and attenuation is the pulse superposition technique or variations of it (Truell et al. [2.2], Fuller et al. [2.4]). A particularly interesting method is the shape resonance technique, also called resonant ultrasound spectroscopy (RUS), suitable for small crystals and low symmetry crystals (Migliori and Sarrao [2.5]). This technique will be discussed together with phase sensitive sound velocity and attenuation measurements in Sect. 2.2. In Sect. 2.3 a short account of phonon echoes will be given. In Sect. 2.4 ultrasonics in pulsed high magnetic field will be described. Apart from the low frequency and the ultrasonic regime, sound waves can also be generated in the microwave region (Tucker and Rampton [2.6]). A method which was used for various applications is the excitation of microwave sound at surfaces in microwave cavities. This will be discussed in Sect. 2.6. The excitation and detection of acoustic surface waves SAW will be discussed in Sect. 2.5. Finally, in Sect. 2.7, the Brillouin scattering will be mentioned. Thermal expansion and magneto-striction experiments are important to determine the length changes with temperature or magnetic field. Apart from this they are important thermodynamic functions in their own right. The experimental technique for these quantities and for measuring thermal conductivity will be discussed in Sect. 2.8. We begin with a discussion of ultrasonic transducers in Sect. 2.1.

2.1 Transducer

Several techniques are in use to generate and to detect ultrasonic waves. The most common one is to use piezoelectric transducers. But also magnetostrictive transducers or electromagnetic generation and detection of sound can be used in special cases. A brief review of the different techniques to generate and detect sound waves follows and some review articles where more details can be found are named.

With the strains and stresses defined in Chap. 3, the piezoelectric effect gives a stress–strain electric field relation

$$T_i = c_{ik}\varepsilon_k - e_{ij}E_j \ . \tag{2.1}$$

Here we use already the contracted Voigt notation, see Sect. 3.1 ($11 \to 1$, $22 \to 2$, $33 \to 3$, $23 \to 4$, $13 \to 5$, $12 \to 6$) for the stress tensor T_{ij} and the strain tensor ε_{ij}. c_{ij} are the elastic constants and e_{ik} the piezoelectric stress coefficients. The inverse relation reads

$$\varepsilon_i = s_{ik}T_k + d_{ij}E_j \tag{2.2}$$

with s_{ik} a component of the compliance tensor. The piezoelectric matrix in contracted notation is given by (e_{ij}) with $i = 1, 2, 3$ (3 directions) and $j = 1, \cdots, 6$ (six components of the stress tensor). For quartz (SiO_2) it has the form

$$[e_{ij}] = \begin{pmatrix} e_{11} & -e_{11} & 0 & e_{14} & 0 & 0 \\ 0 & 0 & 0 & 0 & -e_{14} & -2e_{14} \\ 0 & 0 & 0 & 0 & 0 & 0 \end{pmatrix}$$

with $e_{11} = 0.171C/\mathrm{m}^2$, $e_{14} = 0.0403C/\mathrm{m}^2$ with C dimension of Coulomb (Appendix A). For $\mathsf{LiNbO_3}$ the corresponding components read:

$$[e_{ij}] = \begin{pmatrix} 0 & 0 & 0 & 0 & e_{15} & -e_{22} \\ -e_{22} & e_{22} & 0 & e_{15} & 0 & 0 \\ e_{31} & e_{31} & e_{33} & 0 & 0 & 0 \end{pmatrix}$$

with $e_{15} = 3.65C/\mathrm{m}^2$, $e_{22} = 2.39C/\mathrm{m}^2$, $e_{31} = 0.31C/\mathrm{m}^2$, $e_{33} = 1.72C/\mathrm{m}^2$ (Ogi et al. [2.7]).

For an X-cut quartz an electric field in the x-direction produces a strain in the same direction, therefore producing longitudinal waves. With the parameters for quartz, the longitudinal elastic constant $c_{11} = 8.6 \times 10^{11} erg/\mathrm{cm}^3$, the piezoelectric constant $e_{11} = 0.171\frac{C}{m^2}$ and with a typical applied electric field value of $E_x = 10V/\mathrm{mm}$, the stress is given by $T_1 = e_{11}E_x = 1.71CV/m^3$ and the strain by $\varepsilon_1 = \varepsilon_{xx} = T_1/c_{11} = 0.2 \times 10^{-6}$ – a rather small strain. This would be the maximum strain for a longitudinal sound wave in the x-direction for the typical applied ac electric field. Likewise, shear waves may be generated with a Y-cut crystal. The purest shear mode with a minimum of

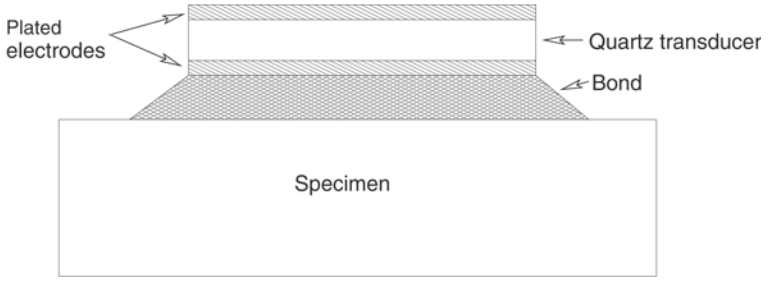

Fig. 2.1. Transducer-Bond-Specimen arrangement

coupling to other modes is the so-called AC-cut quartz crystal, a cut rotated by 31° about the x-axis.

Further details on these transducers can be found in Mason [2.8]. Another transducer material is $LiNbO_3$ with larger piezoelectric coupling constants as shown above. With these transducers, the resonance frequency or odd integer multiples thereof are used.

In addition, there are piezoelectric polymer foils with high efficiency. They can be used non-resonantly over a large frequency range. They are especially suited for longitudinal waves. All these transducers have to be bonded to the specimen with plane parallel polished faces (see Fig. 2.1). Thiokol LP, GE cement, Nonaq or UHU cement can be used as bond materials. If thin film technology is used, transducers, such as ZnO or CdS, can be evaporated or sputtered directly on to the specimen without a bond in between. Details on this fabrication technology can be found in Foster [2.9]. This thin film technique is also important for surface acoustic waves as discussed in Sect. 2.5. Problems arising with the different types of transducers for measuring ultrasonic velocity and attenuation are discussed in Sect. 2.2.

Apart from piezoelectric transducers, there have been studies also on magneto-strictive transducers and on electromagnetic generation of ultrasound. The latter ones have been carried out in metals, ferromagnets and various magnetic materials. Since these techniques have little technical application, no further details are given here but some relevant reviews are: Dobbs [2.10], Buchelnikov and Vasil'ev [2.11], Gorodetsky et al. [2.12].

2.2 Sound Velocity and Attenuation, Experimental Techniques

2.2.1 Simple Ultrasonic Set-Up

A simple ultrasonic system for producing stress waves is now discussed. In Fig. 2.1 we show the transducer–sample system. The (piezoelectric) transducer with electrodes on both sides is bonded to the specimen with parallel

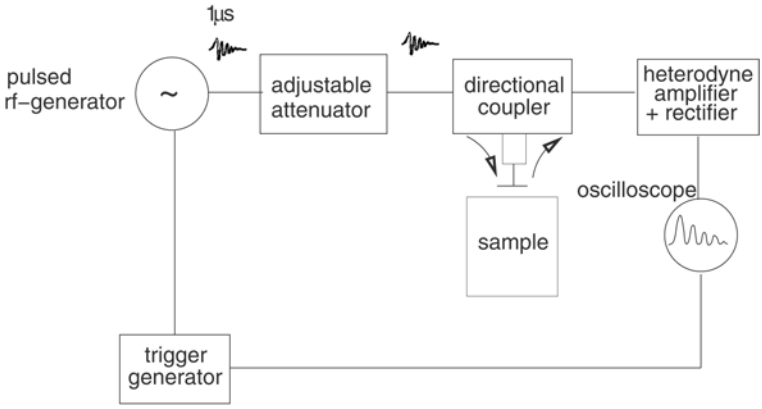

Fig. 2.2. Ultrasonic system to measure sound velocity and attenuation

end faces. For the choice of bond materials see Sect. 2.1. A pulsed electromagnetic signal of $\sim 1\,\mu s$ duration, operating at the fundamental frequency of the transducer or at one of its odd harmonics, is applied across the transducer. With the piezoelectric effect, a stress wave is produced which propagates through the specimen.

In the single transducer arrangement of Fig. 2.2, the same transducer acts as a receiver. Upon reflection on the surface, a small amount of energy is converted back to an electric pulse. The major part of the pulse is reflected and propagates further, producing an ultrasonic echo pattern as shown e.g. in Fig. 2.5a. The converted electric pulse is amplified (with homodyne or heterodyne amplifiers) and shown on the oscilloscope. To investigate a wide frequency range, transducers can be used on both opposite faces of the sample (emitter and receiver) – this does not need a directional coupler. In the following, we discuss phase sensitive devices to measure ultrasonic velocity and attenuation with high accuracy.

A distinction can be made between pulse echo techniques and cw-techniques. In the latter case, the transmitting transducer is driven continuously and a resonant response is observed at frequencies which correspond to $L = n\frac{\lambda}{2}$ with L the sample length and λ the wavelength of the sound. The ultrasonic wave velocity is determined from the resonant frequencies with transducer corrections included. The attenuation follows from the quality factor Q of the resonance signals. In the following, we discuss a special phase-sensitive ultrasonic set-up, absolute sound velocity measurements, the so-called Resonant Ultrasonic Spectroscopy (RUS) and the vibrating reed technique.

2.2.2 Relative Sound Velocity and Attenuation Changes

Of the great variety of experimental techniques mentioned above, we describe an ultrasonic setup used successfully in our laboratory (Heil et al. [2.13], Lüthi et al. [2.14]). It is a slightly changed version of a setup described by Wallace and Garland [2.15]. Our apparatus allows us to perform simultaneous measurements of the ultrasonic velocity $\frac{\Delta v}{v_0}$ and attenuation α as a function of temperature or magnetic field. The frequency range of 5–500 MHz is covered and the duration of the ultrasonic echo pulse is 0.1–1 µs. The repetition rate depends on the available cooling power in the cryostat and lies between 100 Hz in the mK temperature range and a few kHz at higher temperatures. Figure 2.3 shows the electronic part of the ultrasonic setup for the simultaneous detection of ultrasonic velocity changes and attenuation.

With the frequency generator (1) a frequency between 10–500 MHz is chosen, depending on the choice of the transducers. The voltage divider (2) gives the signal for the specimen and for the reference channel. The diode switch (3) triggered by the pulse generator (4) gives a pulse modulated signal with a pulse duration of 0.1–1 µs and a typical repetition rate of 10 kHz. The high frequency pulses amplified with a power amplifier (5) are changed to ultrasonic pulses and vice versa with the transducers on both sides of the sample. The time for a transit through the sample is denoted by τ_0. The different echoes follow the transit signal in time intervals of $2\tau_0$ and with exponentially decaying intensity. Each transit gives a phase shift for the signal of $\Phi = kL_0$. The n-th echo therefore has a phase shift of

$$\Phi_n = kL_0(2n+1) = \frac{\omega}{v} L_0(2n+1) \tag{2.3}$$

with respect to the reference signal. Here k is the wave number of the ultrasound, L_0 the length of the specimen, $\frac{\omega}{2\pi}$ the frequency and v the sound velocity. The received signal is amplified and split into two channels (8). In both mixers (11) a signal from the sample $B = B_0 \cos(\omega t + \Phi_n)$ is multiplied with the reference signal $A_1 = A_0 \cos(\omega t)$ and with the 90° reference signal from the hybrid (10) $A_2 = A_0 \cos(\omega t + \frac{\pi}{2})$. From these expressions

$$A_1 B = \frac{1}{2} A_0 B_0 \left[\cos \Phi_n + \cos\left(2\omega t + \Phi_n\right)\right]$$

and

$$A_2 B = \frac{1}{2} A_0 B_0 \left[\sin \Phi_n + \sin\left(2\omega t + \Phi_n\right)\right]$$

a low pass filter (12) gives the two signals

$$\begin{aligned} I_n &= \frac{1}{2} A_0 B_0 \cos \Phi_n \\ Q_n &= \frac{1}{2} A_0 B_0 \sin \Phi_n \, . \end{aligned} \tag{2.4}$$

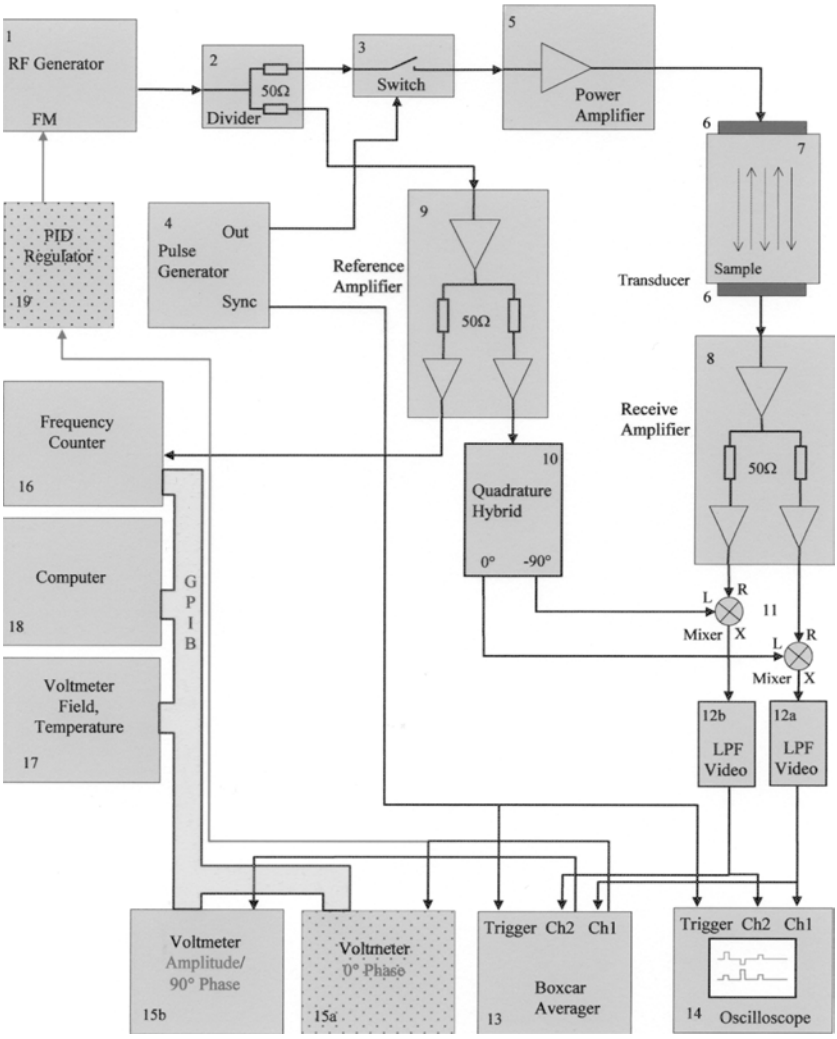

Fig. 2.3. Experimental set up for measuring sound velocity and attenuation. Here we show the apparatus with frequency feedback control. For the quadrature system the feedback loop is missing. For details see text (Lüthi et al. [2.14])

A boxcar (13) reads the two signals. A feedback loop with a PID regulator (19) keeps the phase of the signal I_n constant and changes accordingly the frequency. A computer is used to determine the frequency change and the amplitude of the 90° phase shifted signal Q_n. For the physical interpretation of these results (2.3) is taken into consideration and differentiated to give

$$\frac{\mathrm{d}\Phi_n}{\Phi_n} = \frac{\mathrm{d}\omega}{\omega} - \frac{\mathrm{d}v}{v} + \frac{\mathrm{d}L_0}{L_0} \,. \tag{2.5}$$

With the constant phase, the frequency change is directly proportional to the velocity change. Usually, the length changes due to temperature variation (thermal expansion) or due to magnetic field (magneto-striction) can be neglected in comparison to the velocity changes. The relative accuracy of this method is usually one part in 10^6 for $\frac{\Delta v}{v}$.

For the attenuation measurements, the 90° phase shifted signal Q is taken and the attenuation from the amplitude calculated. This procedure can be carried out for consecutive echoes. A simpler way is to fit echo trains, like the ones shown in Fig. 2.5a, with an exponential, according to the complex parameter k: $u = U \exp i(kx) = U \exp(-\alpha x + ik_r x)$ with $k = k_r + ik_i = k_r + i\alpha$. There are several pitfalls which can make attenuation measurements difficult. Amongst them are coupling losses in the transducers, diffraction effects, misalignment of the single crystal, phonon focusing etc. For a thorough discussion of these different effects see e.g. Truell et al. [2.2].

The attenuation is measured in Np/cm (Neper/cm) or in db/cm (decibel/cm). The relations between these units, with the sound wave amplitude $A(x)$ (see e.g. Fig. 2.2)

$$\text{db/cm} = 20\frac{1}{x_2 - x_1}\log_{10}\frac{A(x_1)}{A(x_2)} \quad \text{and} \quad \text{Np/cm} = \frac{1}{x_2 - x_1}\ln\frac{A(x_1)}{A(x_2)}$$

and therefore db/cm = 8.6859 (Np/cm).

2.2.3 Ultrasonics at Very Low Temperatures

With the advent of top-loading dilution refrigerators, ultrasonics in the milli-Kelvin region became more easily feasible. The exchange of samples could be achieved within a few hours, which is indispensable because of transducer bonding and other problems. Many ultrasonic studies are now performed at temperatures below 1 K. We will discuss the results of such experiments especially in Chaps. 7, 8, 10, 13 and 14.

In Fig. 2.4 we show a schematic plot of a top-loading dilution refrigerator as developed by Oxford Instruments. The cooling power of this system is about 250 mW at 100 mK. Details on $He^3 - He^4$ dilution refrigerators can be found in books on "low temperature physics" as e.g. Pobell [2.16]. It is very important to use efficient ultrasonic transducers for low input power ($LiNbO_3$ or piezoelectric foils). The transducers have to be contacted with very fine 20 µm gold wires. The repetition frequency of the signal has to be as low as possible. With all these precautions, low temperatures below 50 mK can be achieved. For magneto-acoustic experiments, a specimen holder is often needed which can be rotated with respect to the magnetic field direction. The rotation mechanism has to be installed on top of the refrigerator at room temperature. Such a system is described by Wolf [2.17].

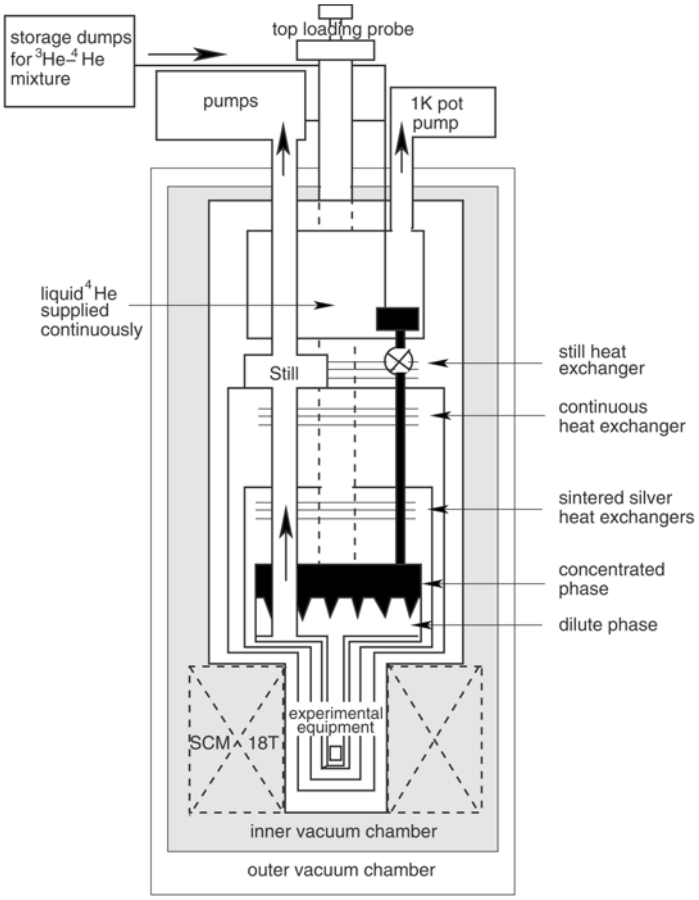

Fig. 2.4. Schematic plot of a top-loading dilution refrigerator as used for different experiments

2.2.4 Absolute Sound Velocity Measurements

An echo train, like the one shown in Fig. 2.5a, is usually taken for measuring the absolute sound velocity, the time interval between different echoes being measured. With the sample length, the velocity $v = L_0 \frac{2n+1}{t}$ can be determined for echo n. Care has to be taken that the starting points of the individual echoes are taken owing to echo shape deterioration. For echoes generated with piezoelectric films, this approach works well, as seen in Fig. 2.5b. For echo generation with transducers of finite thickness, the time delay within the transducer can affect the echo shape, especially for higher echoes. Getting the absolute phase velocity in this case is described in Kim et al. [2.18] and Niksch and Grill [2.19]. In Fig. 2.5a we show echo trains for a sample of URu_2Si_2 (Wolf [2.17]), one using quartz transducer (Fig. 2.5a) and the other using a

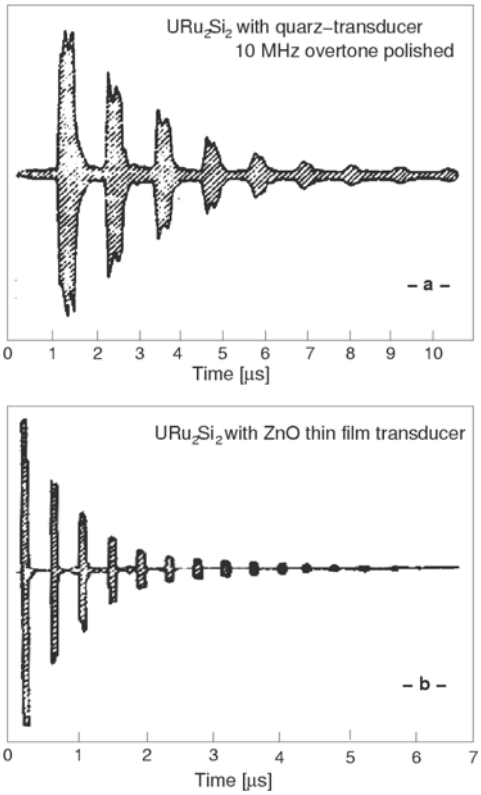

Fig. 2.5. Pulse echo train for ultrasonic waves in URu_2Si_2 (**a**) with Quartz transducers, (**b**) with ZnO–film transducers (Wolf [2.17])

ZnO–film (Fig. 2.5b). The quality difference of the successive echoes in favour of Fig. 2.5b is clearly seen. Another way to determine the absolute velocity is to measure the resonance frequencies of the system sample-transducer and using the relation $v = 2\Delta f L_0(2n + 1)$ where Δf is the frequency change for a phase shift of π for echo n. Phase shifts due to transducers and electronics have to be taken into account too. In all these methods it is necessary to know the length L_0 of the specimen. Furthermore, to convert from sound velocity to elastic constant, the mass density of the crystal must be known. The accuracy of these methods is about 1–3%. For a further sound velocity determination see also below the resonant ultrasound spectroscopy.

In the sound velocity measuring method described above, the phase velocity is measured. There are now new methods using phonon and ultrasonic imaging techniques, where the group velocity is measured, which for an elastic anisotropic medium is generally different in size and direction from the phase velocity. Phonon focusing and internal diffraction effects complicate the picture. This method is a promising tool for the future and can be already

applied not only to insulators with high acoustic Q but also to quite different bulk specimen. An interesting and detailed account of this technique is given in Wolfe [2.20].

2.2.5 Resonant Ultrasound Spectroscopy, RUS

A completely different way to measure absolute sound velocities or elastic constants is the so-called shape resonance technique, also called resonant ultrasound spectroscopy (RUS) (Migliori and Sarrao [2.5]). This method consists of measuring the spectrum of resonance frequencies of a sample and a subsequent solution of the inverse problem of recovering all the components of the elastic constant tensor. In this technique, the plane wave approximation used in pulse echo experiments described above is abandoned. Instead, the normal modes of vibration of a solid specimen of known geometry is used to deduce the complete elastic tensor in a single measurement. The acoustic resonance frequencies can be determined as illustrated in Fig. 2.6. The specimen of known geometry, preferably in a form of a rectangular parallelepiped, is clamped between piezoelectric transducers as shown in the figure. One transducer is used to drive the sample with mechanical vibrations and the other

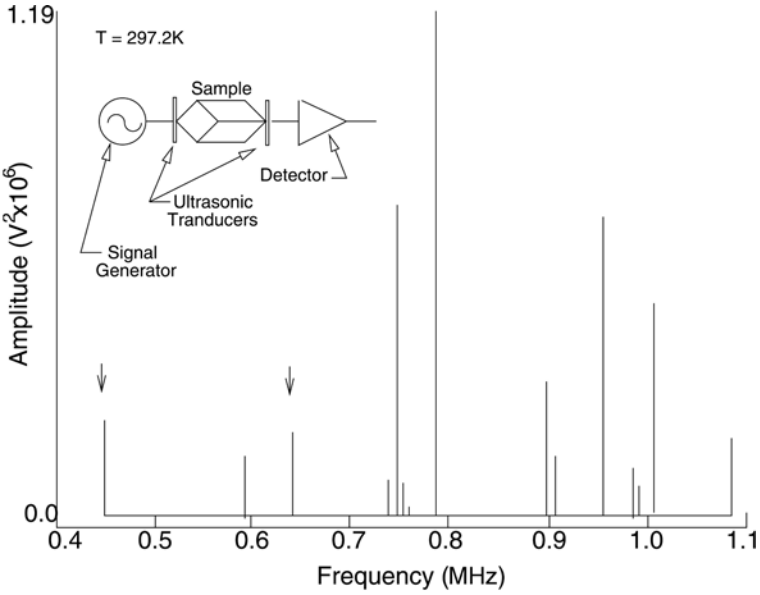

Fig. 2.6. Schematic set-up of the resonance spectroscopy with frequency spectrum (Migliori and Sarrao [2.5])

is used to detect the mechanical response of the sample. A frequency sweep allows a rapid measurement of the resonance modes.

The acoustic resonance frequencies of a single crystal can also be calculated with given dimensions, crystal symmetry, mass density and elastic constants. Via a computational fitting procedure, unknown parameters, e.g. elastic constants, can be determined. With an iterative algorithm, the resonance frequencies calculated analytically can be matched with those measured experimentally. In crystals with a good acoustic Q, resonances ~ 100 in the frequency range of kHz to a few MHz can easily be determined with samples of $\sim$mm dimensions. The fitting procedure gives elastic constant values with an accuracy better than 1%. One of the inaccurate parameters are the length measurements, which can also be included into the fitting procedure.

The great advantage of this method is the possibility of a complete determination of the elastic constant tensor in a single experiment. With pulse echo techniques, it is often necessary to take recourse of propagation directions which are not principal axes and for determining all elastic constants, (for lower symmetry than cubic) different propagation directions are usually required, i.e. often different crystals. This resonant ultrasonic spectroscopy is especially suited for relatively small crystals and for crystal symmetries lower than cubic, where there are more than three elastic constants (see Appendix C). The accuracy of elastic constant determination is high, diffraction and other interference effects are practically absent since there is no plane wave approximation. On the other hand for high accuracy relative elastic constant measurements with a resolution of ~ 1 part in 10^6, the phase sensitive techniques described earlier must be used. In addition, magnetic field dependent effects can only be measured for special field directions with this shape resonance technique. But temperature dependencies of elastic constants have been measured successfully with this technique.

With this new RUS method, the elastic constant tensor of a number of single crystal specimen have so far been investigated – mainly at room temperature: La_2CuO_4 (Migliori et al. [2.21]), $La_{1.86}Sr_{0.14}CuO_4$ (Migliori et al. [2.22]) $YBa_2Cu_3O_{7-\delta}$ (Lei et al. [2.23]), UPt_3, Sr_2RuO_4 (Paglione et al. [2.24]), $LiKSO_4$ and $YD_{0.1}$ (Leisure and Willis [2.25]), piezoelectric $La_3Ga_5SiO_{14}$ (Schreuer [2.26]). Use will be made of some of this data in Chaps. 9 and 10.

The mathematical methods used for this RUS spectroscopy consist of determining the elastic eigenfrequencies and eigenvectors for a simple geometry for a given material. These methods are explained in Migliori et al. [2.27] and Leisure and Willis [2.25]. The starting point is the Lagrangian L, $L = \int_V (KE - PE)\mathrm{d}V$ with $KE = \frac{1}{2}\sum_i \rho(du_i/\mathrm{d}t)^2$ the kinetic energy and $PE = \frac{1}{2}\sum c_{ijkl}\varepsilon_{ij}\varepsilon_{kl}$ the potential energy. Expanding the displacement vector in a complete set of functions $\{\Phi_\lambda\} : u_i = \sum_\lambda a_{\lambda i}\Phi_\lambda$ and substituting into L gives

$$L = \frac{1}{2}\sum \left[a_{\lambda i} a_{\lambda' j} \rho\omega^2 \int_V \delta_{ij} \Phi_\lambda(\boldsymbol{r}) \Phi_{\lambda'}(\boldsymbol{r}') \mathrm{d}V - a_{\lambda_i} a_{\lambda' j} \int_V c_{iji'j'} \Phi_{\lambda,j}(\boldsymbol{r}) \Phi_{\lambda' j'}(r') \mathrm{d}V \right] . \tag{2.6}$$

This expression is written in compact form as $L = \frac{1}{2}\rho\omega^2 \boldsymbol{a}^T \boldsymbol{E}\boldsymbol{a} - \frac{1}{2}\boldsymbol{a}^T \boldsymbol{\Gamma}\boldsymbol{a}$ where the expansion coefficient $\boldsymbol{a}$ is a vector and the integrals in (2.6) are the matrices $\boldsymbol{E}$, $\boldsymbol{\Gamma}$. With L an extremum with respect to the expansion coefficients gives the eigenvalue equation:

$$\Gamma \boldsymbol{a} = \rho\omega^2 \boldsymbol{E}\boldsymbol{a} \, . \tag{2.7}$$

The eigenvalues are $\rho\omega^2$ and the eigenvectors $\boldsymbol{a}$ are the expansion coefficients. Polynomials – Legendre functions depending on the type of crystal and geometric form – are used for the set of functions Φ. There are standard programs to solve such equations. Symmetry arguments and suitable truncation procedure simplify the procedure. Further details can be found in the references given above.

2.2.6 Vibrating Reed Technique

In this technique the sample, a reed, is clamped on one side to a sample holder whereas its free end is electrostatically excited to vibrations. Its motion follows that of a driven oscillator. A second electrode on the other side detects electrostatically the vibrations of the sample. The measurements of the excitation frequency and that of the damping of the oscillator gives the change $\frac{\Delta v}{v}$ of the sound velocity $v = (\frac{E}{\rho})^{1/2}$ or Youngs modulus E and of the internal friction Q^{-1} of solids. The frequency range is typically from 0.1 to 10 kHz. Therefore thermoelastic relaxation effects can be studied together with ultrasound effects over a wide frequency range. Note that a piezo transducer is not needed for this technique. These techniques are described by e.g. Novick and Berry [2.28], Read et al. [2.1], Barmatz and Golding [2.29], Berry and Pritchet [2.30] and Esquinazi [2.31].

For a one ended clamped bar, the vibration frequencies are

$$f_n = \frac{n}{4L_0}(\frac{G}{\rho})^{1/2} \quad \text{and} \quad f_n = \frac{n}{4L_0}(\frac{E}{\rho})^{1/2}$$

with L_0 the length of the bar and for torsional and longitudinal modes respectively and somewhat more complicated expressions for flexural modes (Novick and Berry [2.28]). For a discussion of the elastic moduli E, G, K in an isotropic solid see Sect. 3.4. Experimental results for these low frequency modules are given in Sects. 6.1, 12.2.

2.3 Phonon Echoes

In the seventies and eighties analogous experiments to the nuclear spin echo experiment (Hahn [2.32]) were performed with acoustic waves. In MgO, doped

with Ni^{2+}, echoes were observed with substituting the electromagnetic fields by phonon fields (Shiren and Kazyaka [2.33]). Another class of echo phenomena can be observed in two level systems as they are present in glasses. In such tunneling systems, which can be formally described in analogy to a spin $\frac{1}{2}$ system (pseudo-spin σ), such echo experiments were successfully performed (Graebner and Golding [2.34]). These experiments will be described briefly in Chap. 14. Another class of echo experiments were performed in piezoelectric and non-piezoelectric semiconductors like $LiNbO_3$, SbSI, CdS (Popov and Krainik [2.35], Thompson and Quate [2.36], Billmann et al. [2.37]), also in powder materials (see review articles by Kajimura [2.38] and by Melcher and Shiren [2.39]).

Another echo experiment was also performed with a material exhibiting a structural phase transition using an additional echo material (Fossheim and Holt [2.40]). It can be observed that a backward-wave echo is generated by the interaction of an acoustic wave (frequency ω) with a homogeneous electric field (frequency 2ω) giving a backward wave (frequency ω). This experiment, which is relevant to the physics discussed in Chap. 7, will be discussed in detail in Sect. 7.4.3. For a review of this topic see Fossheim and Holt [2.40].

All the various echo phenomena have the properties of time reversal and phase memory. Apart from the spin echoes mentioned above, photon echoes and, as discussed above, various kinds of phonon echoes have been observed. All echo phenomena are due to nonlinear coupling of the oscillations. As a simple example (Kajimura [2.38]) in a linear system a primary pulse $a\exp(-i\Omega t)$ and a secondary pulse $b\exp[-i\Omega(t-\tau)]$ add up in a superposition of the two pulses. Radiation from systems with many eigenfrequencies Ω gives a response $\sum_\Omega\{a\exp(-i\Omega t)+b\exp[-i\Omega(t-\tau)]\}$ which is essentially zero due to their phase cancellations. No coherent signal is thus produced. But nonlinear coupling gives a coherent echo signal at a particular time, as an example: $\sum_\Omega\{a^\star\exp(i\Omega t)b^2\exp[-2i\Omega(t-\tau)]\}=\sum_\Omega a^\star b^2\exp -i\Omega(t-2\tau)]$ gives a coherent echo signal only for $t=2\tau$.

Apart from the phonon echoes mentioned here, there exist memory echoes in piezoelectric or ferroelectric powders, in powders of ferromagnetic and superconducting metals produced with rf electric fields with extremely long memory times lasting up to days.

2.4 Ultrasonics in Pulsed Magnetic Fields

High Field Apparatus

Before giving details on the ultrasonic set-up in pulsed fields we describe first the apparatus for generating pulsed fields. For a general introduction to pulsed high magnetic fields see e.g. Herlach [2.41] and the series of books by Herlach and Miura [2.42]. In Fig. 2.7 we give a schematic of a pulsed field apparatus as developed by Oxford instruments and installed at the University of Frankfurt (Wolf et al. [2.43]).

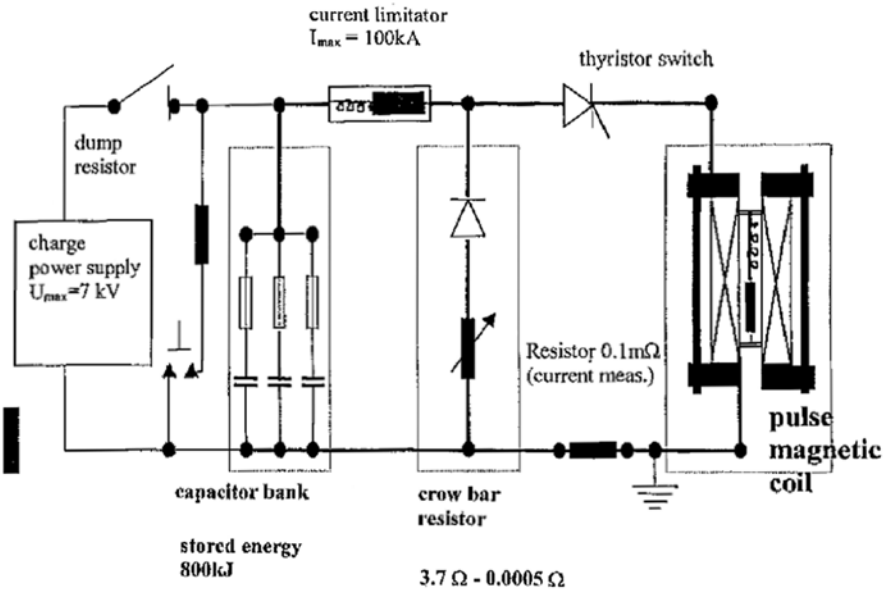

Fig. 2.7. High field apparatus (Oxford instruments)

It is a system for capacitor discharge through a specially designed coil. The capacitor bank has 32mF and the maximum stored energy is about 800 kJ. The discharge is triggered with thyristor switches. A crow bar resistor becomes active when the voltage changes sign, thus dissipating the energy and protecting the capacitors. The 50T coil (developed at the National High Field laboratory in Talahassee) has an inductance of L = 1.81 mH. The high field limitation of this liquid nitrogen cooled coil is not the energy of the capacitor bank but rather the warming up of the coil up to room temperature for a 50 T pulse. The rise time of this coil is about 8 ms and the complete discharge time is about 25 ms. The Copper-wire is reinforced with 1.5% Al_2O_3. Glasfiber together with epoxy resin and a 18 mm steel mantle casing give the necessary mechanical strength. The inner diameter of the coil is 24 mm. It should also be possible to use a 60T coil with this setup. With the inductance L and the capacitance $C = 16\,\mathrm{mF}$, the time for the maximum field $T_{incr} = \frac{1}{4}2\pi\sqrt{LC} = 8.5\,\mathrm{ms}$ is close to the observed one. The decay time with a crowbar resistance ($R = 0.412\Omega$) is approximately $T_{dec} = \frac{2L}{R} = 8.8\,\mathrm{ms}$ instead of 16 ms obtained experimentally because the back flow of current to the capacitor bank was neglected in this estimate.

Ultrasonic System

For experiments in pulsed magnetic fields we use essentially the same setup described in Sect. 2.2 for measuring ultrasonic velocity and attenuation. But

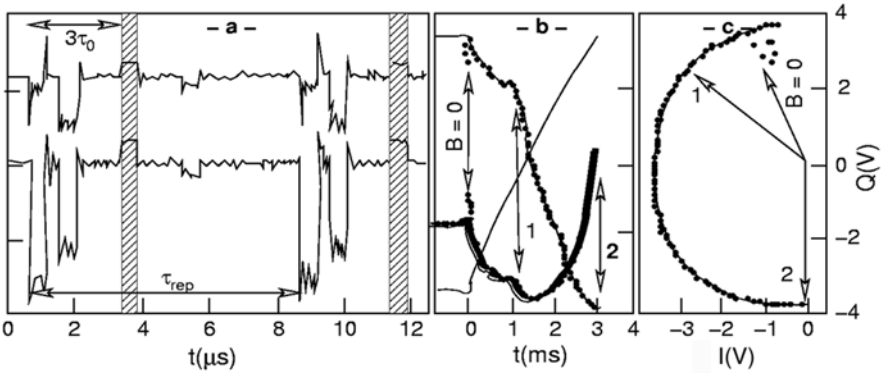

Fig. 2.8. (**a**) Echoes of an ultrasonic experiment, (**b**) t-dependence of I_n, Q_n with magnetic field, (**c**) Vector representation of I_n, Q_n. The arrows in (**b**) and (**c**) mark the same time. The shaded region is the position of the Boxcar gate

the feedback loop described there is too slow to follow the changes of the magnetic field. Therefore all the experiments have to be performed at a fixed frequency and the phase shifts (real and imaginary part) have to be determined numerically (Fig. 2.8). The change in the sound velocity is inversely proportional to the change in the phase (2.3) which must be determined from the data of the two channels:

$$\Phi_n = \frac{\omega}{v} L_0(2n+1) = \arctan\left(\frac{Q_n}{I_n}\right)$$
$$A_n = \sqrt{(I_n^2 + Q_n^2)}\,, \tag{2.8}$$

where A_n is the amplitude of the echo n. In Fig. 2.8 we show the two signals I_n and Q_n for a typical echo pattern.

The repetition rate of the ultrasonic pulses has to be larger in the pulse field experiments. For a pulse length of the high field coil of 20 ms a repetition-frequency of at least 100 kHz is needed. With a standard sampling oscilloscope, 1 point per μs can be taken. Therefore with the repetition frequency given above. there are enough points to measure magnetic field and the two parameters I, Q. The resolution for sound velocity measurements for the equipment in Fig. 2.8 is usually of the order of 10^{-6}. In the pulse field mode this changes to $\sim 10^{-5}$. This homodyne set-up works very well and does not lack in resolution compared to a heterodyne set-up.

Disturbing Factors in Pulsed Magnetic Field Experiments

There are several disturbing factors in ultrasonic experiments with pulsed fields. Heating effects due to eddy currents are the most serious ones. Even for insulating samples care has to be taken with the metalized transducers. By using very thin metal electrodes, this effect can be reduced.

Another disturbing effect is the magneto-caloric effect as it occurs especially near phase transitions. Rough estimates of these disturbing effects can be made by comparing the sound velocity before and just after the pulse with the velocity change as a function of temperature. It is advisable to measure the sample temperature in order to get an estimate of these perturbing factors. For an adiabatic process $\mathrm{d}S = (\frac{\partial S}{\partial T})_B \mathrm{d}T + (\frac{\partial S}{\partial B}]_T \mathrm{d}B = 0$, an infinitesimal field increase $\mathrm{d}B$ leads to a temperature increase $\mathrm{d}T$ of the form $\mathrm{d}T = -(\frac{\partial S}{\partial B})_T / (\frac{\partial S}{\partial T})_B \mathrm{d}B$ and finally (Tishin et al. [2.44])

$$\mathrm{d}T = -\left(\frac{\partial M}{\partial T}\right)_B \frac{T}{C_B} \mathrm{d}B\,, \tag{2.9}$$

where the magnetization $M(T, B)$ and the specific heat $C(T, B)$ are both field and temperature dependent. Equation (2.9) can be integrated from a starting field B_0 to the end field B_e. The magneto-caloric temperature increase is most pronounced for large $(\frac{\mathrm{d}M}{\mathrm{d}T})_B$ and small C. Experimental results of pulsed field ultrasonics are given in Chap. 9 and in Chap. 12. A study of the magneto-caloric effect in pulsed fields will be given in Sect. 12.1.1. Note that the magneto-caloric effect is disturbing measurements in pulsed fields under adiabatic conditions. On the other hand this effect has different important applications as e.g. producing low temperatures by magnetic refrigeration machines and for very low temperatures ($T < 1\,\mathrm{K}$) by the adiabatic demagnetization process, or for characterising phase transitions.

2.5 Surface Acoustic Wave Generation and Detection

Surface acoustic waves (SAW) are important in seismology, in non-destructive testing and especially in signal processing in electronic systems. The low acoustic velocity compared to the light velocity, together with the corresponding small acoustic wavelength make it possible to gain a reduction in size and weight compared to electromagnetic devices. There are many devices possible for signal processing applications such as delay lines, bandpass filters, ultrahigh frequency oscillator control elements, programmable devices for frequency and time domain filtering, frequency synthesizers and correlators etc. Apart from these technical devices, SAW also have many applications in solid state physics as shown in later chapters. The physical properties of SAW propagation, especially the so-called Rayleigh waves, will be presented in detail in Sect. 3.5.

Surface waves can be generated in quite different ways. Usually the same method can be used also for detection. There exist several reviews covering the different methods of generating and detecting SAW (White [2.45], Dransfeld and Salzmann [2.46], Oliner [2.47]). Here we briefly discuss the widely used single phase array and inter-digital SAW transducers, the latter one being the most fundamental component for SAW generation. A more detailed account can be found in the listed reviews.

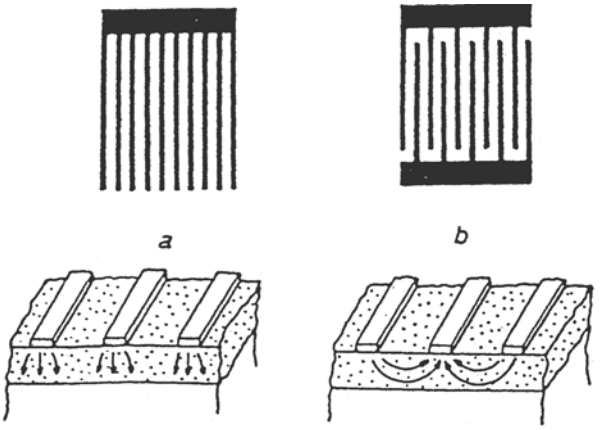

Fig. 2.9. Electrode structures for generation and detection of SAW: (**a**) single array, (**b**) inter-digital array

Figure 2.9 shows the electrode structure for SAW generation and detection. Consider a plane substrate: at the place of the structure, a thin metallic film as counter electrode and on top of it a piezoelectric film (CdS or ZnO) is evaporated or sputtered onto the substrate and finally the electrode structure is placed as shown in the figure. This structure is patterned lithographically. An electric field between the electrodes leads to strains in the piezoelectric layer and to the substrate. The field distribution in the layer is also shown in Fig. 2.9a,b for the two electrode-structures. Denoting with d the distance between two neighbouring stripes in the single phase array, the SAW velocity is $v_S = d\,f$, where f is the frequency of the hf field. The SAW has a wavelength λ with $d = n\lambda$, n integer. It radiates perpendicular to the structure in both directions. The inter-digital transducer has a higher efficiency than the single phase array. The possible frequency range of SAW generation and detection covers typically from 50 MHz to 5 GHz.

The wider field of surface phonons, i.e. not only low frequency and low k-vector, but the whole k range to the Brillouin zone can be investigated with different techniques: energy loss spectroscopy, scattering with He atoms. Reviews on these different techniques by Toennies and Ibach can be found in Kress and de Wette [2.48]. Applications of SAW to solid state physics problems will be given in Sects. 3.5, 6.2, 9.2, 10.6, 13.5 and 13.6.

2.6 Microwave Ultrasonics

If the sound wave frequency is increased up to the microwave frequency, say 10 GHz, the acoustic wavelength becomes very small. With a typical sound velocity of 5 km/s, the wavelength for 10 GHz is 5000 Å. This makes

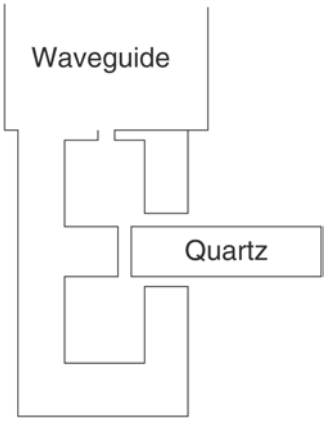

Fig. 2.10. Re-entrant co-axial resonant cavity used with a delay quartz crystal transducer

resonant ultrasonic emission and detection very difficult. Therefore a non-resonant method, using a surface generation is employed. The gradient of the piezoelectric stress is largest at the crystal surface and hence the ultrasonic longitudinal wave is (Jacobsen [2.49])

$$u_L = \frac{e_{11}E^0}{kc_{11}} \sin(\omega t - kx)$$

with e_{11} the piezoelectric stress constant and E^0 the amplitude of the microwave electric field.

The experiment is usually carried out with a re-entrant resonant cavity (Fig. 2.10). With the small wavelength quoted above, the crystal surfaces have to be flat and parallel within optical quality. In addition the microwave sound attenuation can be very high. Therefore only experiments with high acoustic quality crystals have been performed. With the cylindrical re-entrant microwave cavity a strong electric field at the polished end face of the sample is generated (Fig. 2.10) which leads, for instance, to a longitudinal stress (2.3) $T_{xx} = c_{11}\varepsilon_{xx} - e_{11}E_x$ and to a sound wave of the form given above (Jacobsen [2.49]). The first groups performing such experiments in the GHz range were Baranskii [2.50], Jacobsen [2.51] and Bömmel and Dransfeld [2.52], [2.53]. The latter group studied Quartz at 1 GHz. Pomerantz [2.54] used ferromagnetic films as transducers and studied at 9 GHz a number of high quality single crystals of CdS, GaAs, Ge, Si, CaF_2, Al_2O_3 and MgO. Lange [2.55] investigated rutile at 1 and 3 GHz and King and Rosenberg [2.56] performed experiments at 1 GHz in InSb and GaAs. The highest microwave acoustic frequency achieved with this cavity technique is 114 GHz in quartz (Iluker and Jacobsen [2.57]).

A detailed account of these types of experiments and what can be learned about phonon processes is given by Tucker and Rampston [2.6], Beyer and

Letcher [2.58] and Truell et al. [2.2]. Since, for the reasons listed above, the number of experiments and the number of investigated compounds is rather limited and since these experiments are widely discussed in the quoted monographs, only occasionally reference will be made to these and related experiments (Sects. 4.2.2, 5.5, 11.2, 13.3 and 13.4).

There are various different developments in microwave or more general high frequency ultrasonics. A widely known technique is the use of superconducting tunneling junctions as phonon generators and detectors as first shown by Eisenmenger and Dayem [2.59]. Depending on the superconducting tunnel junction, phonon experiments can be performed in a wide frequency range 70–800 GHz. For reviews on these techniques see Eisenmenger [2.60], Kinder [2.61]. Another widely used method is to produce heat pulses from metal films on insulators. The metal film may be ohmically heated with an electric current or optically heated with a laser beam. While many experiments, like phonon focusing and phonon imaging, were performed with such techniques, they lie outside the scope of this investigation. A good account of these techniques, mentioned already in Sect. 2.2 with many references, is Wolfe [2.20].

2.7 Brillouin Scattering

The wavelength of visible light is much larger than the lattice constants. Therefore in an ideal crystal, light can only be scattered by lattice vibrations or other elementary excitations. The scattering of light from acoustic phonons is called Brillouin scattering – from optic phonon branches it is the Raman scattering. Energy and momentum conservation laws give $\hbar\omega' = \hbar\omega \pm E_q$ and $\boldsymbol{k'} = \boldsymbol{k} \pm \boldsymbol{q}$ with E_q the excitation energy of momentum q for a collective excitation, ω and ω' are the laser frequencies of the incoming and scattered light. For a given scattering geometry $(\boldsymbol{k}, \boldsymbol{k'})$, the frequency change $\omega' - \omega$ is measured interferometrically. The frequency changes measured conveniently lie in the GHz region. They are therefore complementary to the ultrasonic waves. There are now very sophisticated Brillouin-scattering apparatus available for transparent and opaque materials. Figure 2.11 shows an apparatus for 180° geometry (Sandercock [2.62]). The techniques are described in review articles (Pine [2.63], Sandercock [2.62]). For high resolution a Fabry–Perot interferometer is used. This device will transmit light of wavelength λ if the spacing L of the two mirrors is $L = m\frac{\lambda}{2}$ with m an integer. The ratio of maximum to minimum transmission, called the contrast of the interferometer, can be improved by placing two or more interferometers in series. A more elegant method is to pass the light two or more times through the same interferometer. For the design of such a multi-pass interferometer see Sandercock [2.62].

The Brillouin scattering technique being based on statistical data collection cannot have such a high resolution as the phase-sensitive ultrasonic

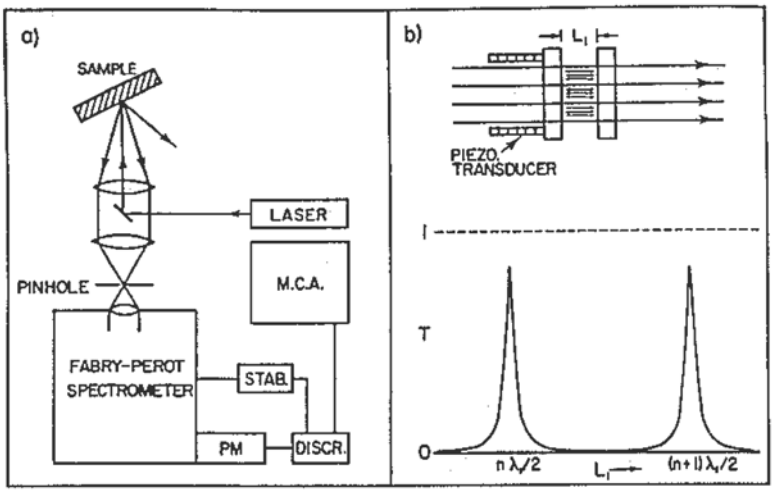

Fig. 2.11. (**a**) Experimental set-up for backscattering with a Fabry–Perot multipass spectrometer. PM photomultiplier, M.C.A. Multichannel analyser, (**b**) transmission of monochromatic light by scanning Fabry–Perot interferometer (Sandercock [2.62])

methods for velocity measurements discussed above. But its frequency range is in the Gigahertz region. Furthermore the method is contact free, a great advantage for many compounds. In the following we will use various Brillouin scattering results in addition to ultrasonic results. Examples are given in Sects. 7.2.2, 9.2, 10.4, 11.2.5, 12.6 and 13.5.

Using Brillouin scattering with a 180° backscattering geometry, Mock and Güntherodt [2.64] showed that bulk modulus and elastic constants can be determined for both metallic polycrystalline samples and single crystals. For a small penetration depth of the light, the spectrum consists of the SAW Rayleigh mode $\omega_R = v_R q_{//}$ and the longitudinal mode $\omega_L = v_L q_{//}$. These two modes determine the elastic moduli c_L, c_T and c_B for a polycrystalline metal. For single crystals various crystal directions can be used to get a complete set of elastic constants. For examples, see the references given above. Unlike the microwave phonon technique (Sect. 2.6) for the Brillouin scattering, the extreme high quality factors for the surface do not need to be considered. Therefore, the range of applications as far as materials are concerned, is much larger than for microwave ultrasonics, the relative accuracy is however lower as discussed above.

2.8 Thermal Expansion and Magneto-striction, Thermal Conductivity

2.8.1 Thermal Expansion and Magneto-striction

Length changes of specimen are important to know for making possible corrections for physical properties. This is especially true for compounds with giant magneto-elastic coupling constants, like heavy rare earth metals or the rare earth-iron Laves phase compounds RFe_2 (see Sect. 5.4). But thermal expansion and magneto-striction are also important thermodynamic derivatives, giving the same coupling constants as gained from elastic constant measurements. As a first derivative of the thermodynamic potential the coupling constants enter linearly (giving the sign) and not quadratically like for elastic constants.

For measuring relative length changes, a variety of different techniques can be used: strain gauges, interferometric methods, double grating with photocell arrangements and capacitive methods (White [2.65], Brändli and Griessen [2.66], Ott and Lüthi [2.67], Lang [2.68]). The most widely used method now is the capacitive method. It has the advantage of high accuracy even with small samples and it can be used without corrections in external magnetic fields. Therefore it is suitable for the study of both thermal expansion and magneto-striction, especially at low temperatures. Capacitance bridges of high sensitivity are commercially available (e.g. General Radio, Type 1615-A). Figure 2.12 shows a schematic drawing of a sample holder used for capacitive length measurements (Ott and Lüthi [2.67]). Such a capacitance dilatometer has a sensitivity of the order of 10^{-9} for relative length changes. It is therefore ideally suited for many applications such as length change corrections for elastic constant measurements, thermal expansion anomalies near phase transition temperatures, study of lattice effects of different phase transitions, etc.

Apart from corrections to sound velocities, the thermal expansion and magneto-striction results are discussed in Sects. 5.2, 9.2, 10.7 and Chap. 6. A thorough discussion of magneto-striction in ferromagnetic substances is given by de Lacheisserie [2.69].

2.8.2 Thermal Conductivity

Since thermal conductivity is discussed in several places (Sects. 4.5, 12.4) some remarks on the experimental techniques for measurements are in order. The thermal conductivity coefficient κ relates the heat flux $\frac{\mathrm{d}\boldsymbol{Q}}{\mathrm{d}t}$ and the temperature gradient by Newton's law $\frac{\mathrm{d}\boldsymbol{Q}}{\mathrm{d}t} = -\kappa\nabla T$. κ therefore has the dimension Watt/Km. To determine a tensor component of κ one usually takes a steady state method. The temperature difference ΔT along a bar of material is measured using thermocouples. ΔT varies typically about 1% of the absolute temperature, which is stabilised for each data point. Measuring $\frac{dQ}{\mathrm{d}t}$

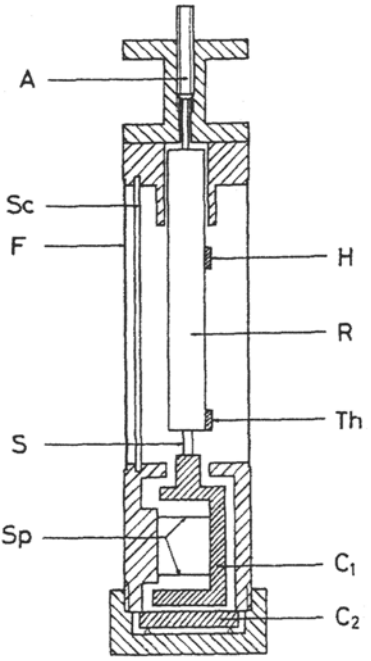

Fig. 2.12. Capacitance dilatometer: Schematic drawing of sample holder. A screw to adjust capacitor gap, C_1, C_2 capacitor plates, F copper frame, H heater, R copper rod, S sample, Sc screw fixing copper frame, Sp springs, Th thermometer (Ott and Lüthi [2.67])

of the heater and ΔT gives the thermal conductivity coefficient. The method has usually an accuracy of $< 5\%$. Details for this method can be found in Brüesch [2.70] and Berman [2.71].

http://www.springer.com/978-3-540-72193-2

Physical Acoustics in the Solid State
Lüthi, B.
2005, XIII, 428 p., Softcover
ISBN: 978-3-540-72193-2